

Transient Superconductivity far above T_c in Light-stimulated $\text{YBa}_2\text{Cu}_3\text{O}_{7-\delta}$

S. Kaiser^{1,*}, D. Nicoletti^{1,*}, C.R. Hunt^{1,4}, W. Hu¹, I. Gierz¹, H.Y. Liu¹, M. Le Tacon²,
T. Loew², D. Haug², B. Keimer², and A. Cavalleri^{1,3}

¹ *Max Planck Department for Structural Dynamics, Hamburg, Germany*

² *Max Planck Institute for Solid State Research, Stuttgart, Germany*

³ *Department of Physics, Oxford University, Clarendon Laboratory, Oxford, United Kingdom*

⁴ *Department of Physics and the Frederick Seitz Material Research Laboratory, University of
Illinois at Urbana-Champaign, Urbana, Illinois 61801, USA*

Strong optical fields at THz frequencies, capable of dynamically deforming the crystallographic structure of a solid, are a new tuning parameter for complex condensed matter. We use mid-infrared femtosecond pulses to resonantly excite large-amplitude vibrations of the apical oxygens in underdoped $\text{YBa}_2\text{Cu}_3\text{O}_{7-\delta}$. A transient superconducting state is discovered for base temperatures far above T_c . A finite superfluid density is observed up to room temperature, evidenced by a characteristic $1/\omega$ frequency dependence in the imaginary part of the optical conductivity σ_2 . Gapping in the real part σ_1 and a short-lived Josephson plasma edge along the c -axis are further evidence of a light induced superconducting state. Our experiments open tantalizing prospects for optically-driven superconductivity in new regions of the cuprate phase diagram or in new materials.

Many experimental findings suggest that underdoped cuprates retain important properties of a superconductor at temperatures above the transition temperature T_c ^{i,ii,iii}. Unlike in BCS superconductors, the loss of long-range phase order is one of the key elements determining the transition temperature in the cuprates^{iv}. Hence, if the order-parameter phase could be stabilized either by design^v or by external stimulation^{vi}, superconductivity may become observable at temperatures above the equilibrium T_c .

In this paper, we report on the use of coherent optical excitation to induce a transient superconducting state in $\text{YBa}_2\text{Cu}_2\text{O}_{7-\delta}$ far above the equilibrium transition temperature T_c . We exploit the technique of mid-infrared control of lattice distortions^{vii,viii,ix}, an important addition to optical techniques at near visible wavelength, which have been used in the past to investigate quasi-particle dynamics^{x,xi,xii,xiii,xiv,xv,xvi} or to enhance superconductivity by charge injection^{xvii,xviii}. Here, femtosecond mid-infrared optical pulses were used to modulate the position of the apical oxygen atoms in the direction normal to the superconducting planes (see Fig. 1).

Two underdoped compounds were studied, $\text{YBa}_2\text{Cu}_3\text{O}_{6.6}$ (YBCO 6.6) and $\text{YBa}_2\text{Cu}_3\text{O}_{6.5}$ (YBCO 6.5), corresponding to hole doping levels of 11% and 9% and exhibiting superconducting transition temperatures $T_c=62$ K and $T_c=50$ K, respectively. The samples were cut and polished along the ac -direction and were characterized by SQUID as well as by measuring their equilibrium THz optical properties (see supplementary information S1).

Mid-infrared pulses at $\sim 15\text{-}\mu\text{m} \pm 2 \mu\text{m}$ wavelength (20 THz, 660 cm^{-1} , 83 meV, $\pm 15\%$), resonant with the infrared active distortion shown in Figure 1, were generated by difference-frequency mixing in an optical parametric amplifier

and focused to a maximum fluence of 2 mJ/cm² with polarization perpendicular to the superconducting planes.

The time-dependent optical properties were probed by time-domain THz-reflectivity for frequencies between 0.5 and 2.5 THz in both samples. Single-cycle probe pulses were generated by optical rectification of a near-infrared (800-nm wavelength) femtosecond pulse in a ZnTe crystal. Detection of the reflected THz field was achieved by electro-optical sampling in a second ZnTe crystal.

Figure 2 displays representative results for photo-stimulated YBCO 6.6. In Fig. 2A, we plot the change of the reflected probe field polarized in-plane, measured at 2.5-ps pump-probe time-delay for temperatures of 80, 280, and 300 K.

From these differential measurements, and from the equilibrium conductivity $\sigma_1^0(\omega) + i\sigma_2^0(\omega)^{\text{ix}}$, we extracted the frequency- and time-delay-dependent conductivity $\sigma_1(\omega, \tau) + i\sigma_2(\omega, \tau)$. In all the experiments the conductivity was calculated by numerically solving Maxwell's equations, accounting for the inhomogeneous exponential depth profile of the pump field, which decays over 4 μm into the sample. In the case of in-plane probing (Figs. 2 and 3), as the penetration depth of the probe pulse is below 2 μm for all frequencies and temperatures measured, almost identical results could be obtained by assuming a homogeneously excited semi-infinite bulk volume (see supplementary material S2 and S3).

In Figure 2B, the imaginary part of the conductivity, σ_2 , is displayed for these three representative temperatures at 2.5 ps pump-probe time delay (blue dots). The imaginary conductivity at equilibrium (grey line) is reported in the

same figure. A characteristic $1/\omega$ frequency dependence in the light-induced state can be clearly seen for all temperatures up to approximately 280 K. This frequency dependence is indicative of a perfect conductor down to frequencies below 0.5 THz, and is the first indication of transient superconductivity^{xx}.

The black dashed lines are fits to the transient conductivity, obtained using the function $\sigma_2(\omega, \tau) = \frac{D^{SF}(\tau)}{\omega} + C(\tau) + \sigma_2^0(\omega)$. In this expression, $D^{SF}(\tau)$ is equivalent to $\lim_{\omega \rightarrow 0} \omega \sigma_2(\omega, \tau)$, and is taken as proportional to the transient superfluid density. The frequency-independent term $C(\tau)$ takes into account all incoherent contributions, for example from quasi-particles heated by the pump field or from lattice deformations (see supplementary material S4). Importantly, for all temperatures below ~ 230 K, the transient conductivities could be fitted using the superconducting component alone $\sigma_2(\omega, \tau) = \frac{D^{SF}(\tau)}{\omega} + \sigma_2^0(\omega)$, and assuming $C(\tau) = 0$ for all time delays. For the highest temperatures ($T > 230$ K), we could only fit the data including the constant term.

In the surface plot of Figure 2C we summarize the result of these fits for all time delays. Perfect conductivity appears within 2 ps after optical excitation and relaxes within a few tens of picoseconds.

In Figure 3, we report similar measurements in YBCO 6.5, organized along the same lines. As in YBCO 6.6, a transient state with similar optical properties is observed up to comparable temperatures.

Corroborating evidence for light-induced superconductivity was found when analyzing the time-dependent $\sigma_1(\omega, \tau)$, as displayed on the left hand side of

Figure 4 for the two doping levels. A large reduction in $\sigma_1(\omega)$ is observed, indicating gapping and confirming the formation of a transient superconductor. In the panels on the right-hand side we display the dynamics of the partially integrated spectral weight, $SW(\tau) = \int_{0.7 \text{ THz}}^{2.3 \text{ THz}} \sigma_1(\omega, \tau) d\omega$, which reduces and recovers on the same timescale as the superfluid density $D^{SF}(\tau)$ increases and decreases back to zero. This effect remained observable up to the same temperature scales for which nonzero D^{SF} was extracted from the fits to $\sigma_2(\omega, \tau)$, as discussed in the supplementary material (see S5).

Figure 5 displays the out-of-plane reflectivity in the light-induced state (calculated according to the procedure discussed in S3), which is characterized by the appearance of a transient reflectivity edge similar to the one observed when cooling below T_c . The edge appears about 1 ps after photo-excitation and then relaxes on a 3-ps timescale. This feature, typically referred to as the Josephson plasma edge, originates from the inductive-capacitive coupling between the planes^{xxi} and is observed in the c -axis optical properties of superconducting cuprates at equilibrium^{xxii,xxiii,xxiv}. Analysis of the out of plane conductivity change, displayed in the supplementary material S3 (figure S3.2), shows the same gapping of $\sigma_1(\omega, \tau)$, and $1/\omega$ divergence of $\sigma_2(\omega, \tau)$, reported in figures 2 and 3 for the in-plane data.

These photo-induced changes show a resonant behavior when the pump wavelength is tuned towards the apical oxygen mode, as reported in previous experiments involving optical excitation of vibrational resonances.

A quantitative interpretation starts from the fits to the in-plane imaginary conductivity. In Figure 6A we plot D^{SF} as a function of base temperature, displayed in an inverse scale. For all temperatures, the light-induced

superfluid density D^{SF} in YBCO 6.6 is higher than in YBCO 6.5, suggesting that at a higher density of holes a “stiffer” superconductor can be created. The non-equilibrium superfluid density is observed to remain nonzero up to a temperature scale $T' \gg T_c$, although at these highest temperatures the density drops by nearly two orders of magnitude compared to that measured in the equilibrium superconductor at 10 K^{xxv}.

The temperature dependence is well fitted by the phenomenological functional form, $D^{SF} = A e^{\frac{\Delta}{kT}} \tanh\left(1.69 \sqrt{\frac{T'}{T} - 1}\right)$, which includes both a BCS gap equation^{xxvi,xxvii} often used in the cuprates^{xxvii,xxviii}, and an exponential term $A e^{\frac{\Delta}{kT}}$, which indicates activated depletion across a temperature independent gap $\Delta = kT'$ ^{xxix,xxx}. Note that this phenomenological fitting function, which diverges for $T \rightarrow 0$, is only valid for $T > T_c$.

Remarkably, a single temperature scale T' is used for both gaps, yielding $T'_{6.6} = 285 \pm 20$ K and $T'_{6.5} = 290 \pm 50$ K.

In Figure 6B we draw a schematic phase diagram, which highlights the region over which non-equilibrium superconductivity is achieved. More than one class of explanations can be invoked for our observations.

Firstly, excitation of the lattice may be an effective mean to “melt” a competing ordered state that might suppress T_c . In the stripe-ordered compound $\text{La}_{1.675}\text{Eu}_{0.2}\text{Sr}_{0.125}\text{CuO}_4$, vibrations in the plane were effective in melting a competing phase and in making transient superconductivity emerge^{xxxi}. However, in the present case the excitation of the apical oxygen is not easily related to any structural distortion that depresses superconductivity, and the underlying structural path would have to be along

more than one normal coordinate^{xxxii}. In such a “competing order melting” view, one could interpret the 20-ps-long relaxation time, which is about two orders of magnitude larger than the 300-fs long excitation pulse, as a relaxation from a metastable superconducting state protected by a kinetic barrier. Experiments that make use of fast femtosecond probes to interrogate charge and spin order, for example using scattering with a free electron laser^{xxxiii}, may clarify the underlying physics.

Secondly, as observed experimentally when correlating the local electronic structure of some cuprates to the position of the apical oxygen^{xxxiv}, and as discussed theoretically^{xxxv,xxxvi,xxxvii}, we speculate that the super-exchange coupling and the pairing gap may be enhanced, on average, by the modulation impressed onto the Cu-O_{apical} bond, which for the 2-MV/cm field strengths used here can be estimated to be as large as 7 pm (see supplementary material S6). Coherent transport may be enhanced in this way for times immediately following optical excitation.

Finally, more exotic explanations can be invoked. We recall how dephasing in various physical systems can be inhibited by rapid modulation, as observed in classical mechanics^{xxxviii,xxxix} or in Nuclear Magnetic Resonance^{xl}, to mention only two of the most striking examples. As the 20-THz modulation used here occurs at frequencies high compared to plasma excitations between planes, one could envisage a dynamically stabilized stack of Josephson coupled planes.

In our experiment, we establish a new temperature scale $T' \gg T_c$. One natural question to be posed pertains to the relation between T' and other temperature boundaries found when measuring physical properties of

underdoped cuprates, such as the pseudogap temperature T^* or the temperature up to which phase fluctuations are observed, T_{Nernst} . We have noted that the temperature-dependent superfluid density of the light induced state has a clear exponential decrease. This may be related to the nature of the incoherent state before excitation. Such temperature dependence is compatible with the ground state acting as a reservoir that is susceptible to light-induced formation of a coherent state, where the “density” of this reservoir reduces as the temperature is increased.

Although the superfluid density of the light-induced state reduces with base temperature, the frequency of the plasma edge remains high at all temperatures, comparable to the one observed at equilibrium below T_c . This observation is incompatible with a homogeneous light-induced state, for which one would expect a frequency of the Josephson edge decreasing with the average D^{SF} . A useful analogy to explain this observation would be an inhomogeneous system in which islands of “dense” superconductivity are created by the light pulse. In the planes, grains with high superfluid density (and low equivalent inductance) would then be “in series” with regions of low superfluid density (and high inductance), leading to a low average density (or high total inductance). On the contrary, the out of plane response would be dominated by tunneling between high superfluid density regions (low equivalent inductance), which would “short” all other couplings.

In summary, we have used vibrational control in the mid-infrared to induce transient superconducting transport in underdoped cuprates. Three different observations substantiate this conclusion. Firstly, the in-plane imaginary conductivity exhibits a $1/\omega$ scaling, providing a direct proof of collision-less

transport. Secondly, the in-plane real part of the conductivity loses spectral weight, as expected in a superconductor. Thirdly, the out-of-plane reflectivity shows the appearance of a Josephson plasma edge at approximately the same frequency as that observed below T_c . These phenomena survive up to temperatures far above T_c , indeed near room temperature, presenting a new, vivid demonstration of the importance of high temperature scales in cuprates. A grand challenge for future research is to encapsulate our findings in a new class of theories that can describe the physics of optically modulated cuprate superconductors. Experimentally a more immediate goal will be to optimize strength, bandwidth, and duration of the optical stimulation, to stabilize coherent states on timescales long compared to the 20-30 ps observed in this work. Achieving this would open exciting prospects for optically driven DC superconductors.

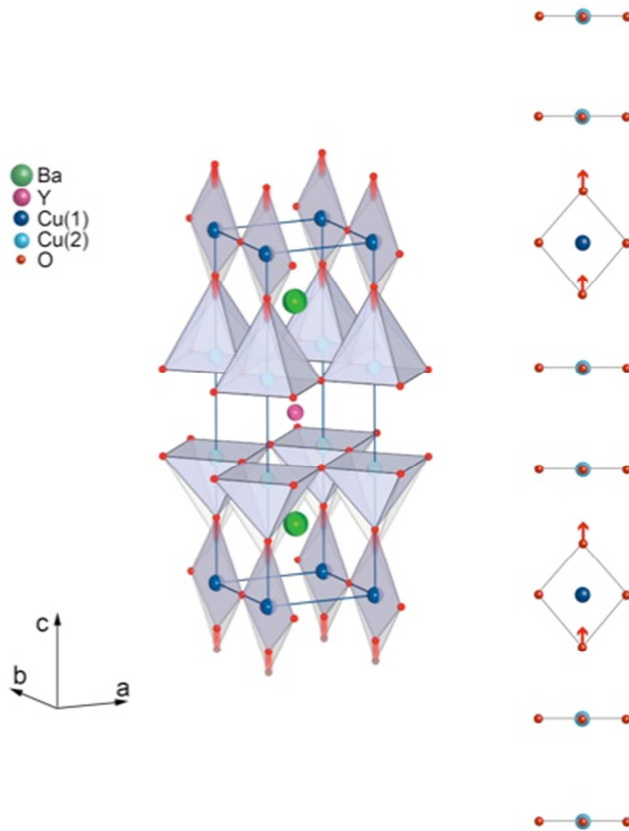


Figure 1. Structure of $\text{YBa}_2\text{Cu}_3\text{O}_{7-\delta}$ and lattice distortion for the 20 THz mode. Two conducting CuO_2 planes (Cu(2), and O in the ab -plane) are separated by Y atoms (pink) and form a bi-layer unit. Ba atoms (green) and the CuO_4 ribbons (Cu(1), and O in the bc -plane) separate bi-layer units^{xli}. The excitation of the infrared-active B_{1u} mode at $15\text{-}\mu\text{m}$ wavelength drives only the displacement of the apical oxygen atoms in the ribbons along the c direction^{xlii,xliii}.

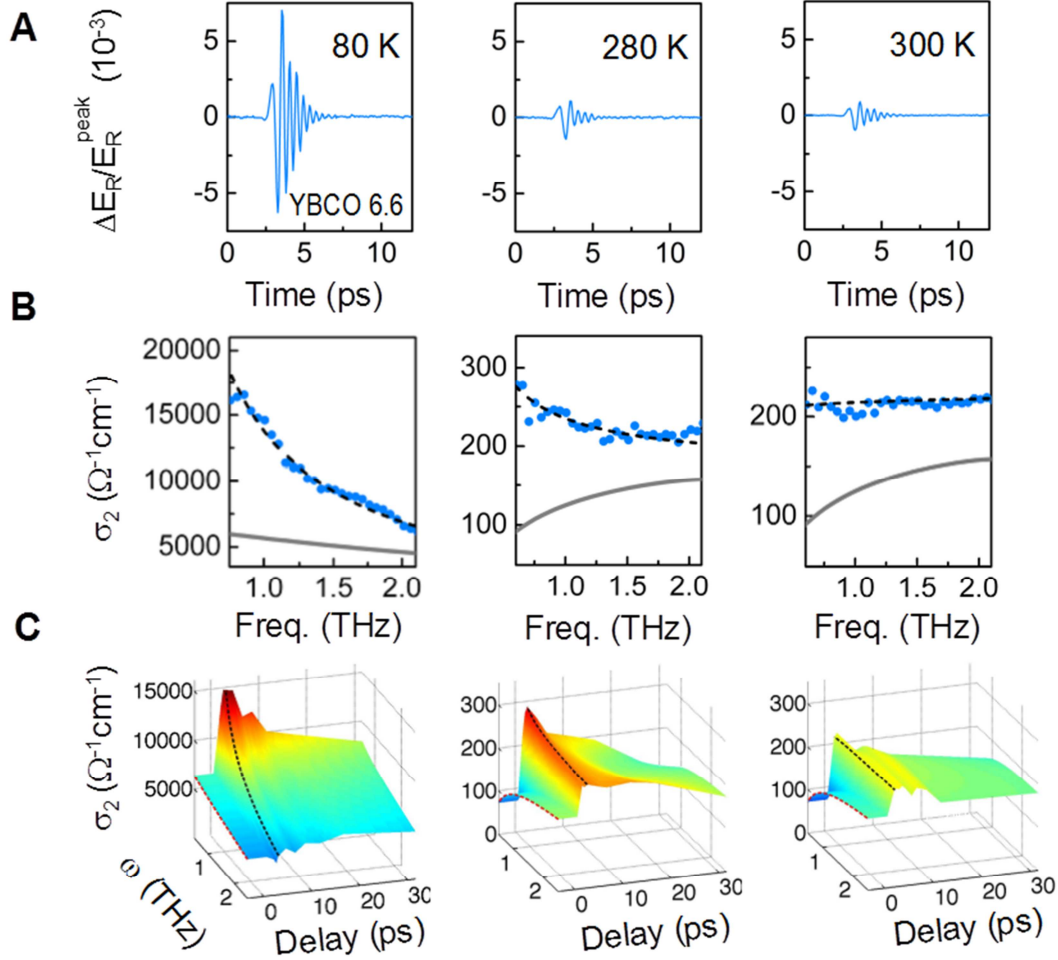


Figure 2. (A) Differential field reflectance ($\Delta E_R/E_R^{peak}$) in photo-stimulated YBCO 6.6, at three different temperatures above T_c (80 K, 280 K, 300 K), measured with THz pulses polarized along the a -axis (perpendicular to the CuO chains). The spectra are taken 2.5 ps after excitation with a 15 μm pulse polarized along the c -axis. (B) Imaginary part of the optical conductivity, σ_2 , as extracted from the amplitude- and phase-resolved reflectance using a multilayer model (see supplementary material S2 and S3). Black dashed lines are fits to the measured data with the function $\sigma_2(\omega) = \frac{D^{SF}}{\omega} + C + \sigma_2^0(\omega)$, where D^{SF} and C are frequency-independent constants that vary with time delay. The grey line shows $\sigma_2^0(\omega)$, the equilibrium conductivity at negative time delays^{xix}. (C) Time and frequency dependence of $\sigma_2(\omega, \tau)$.

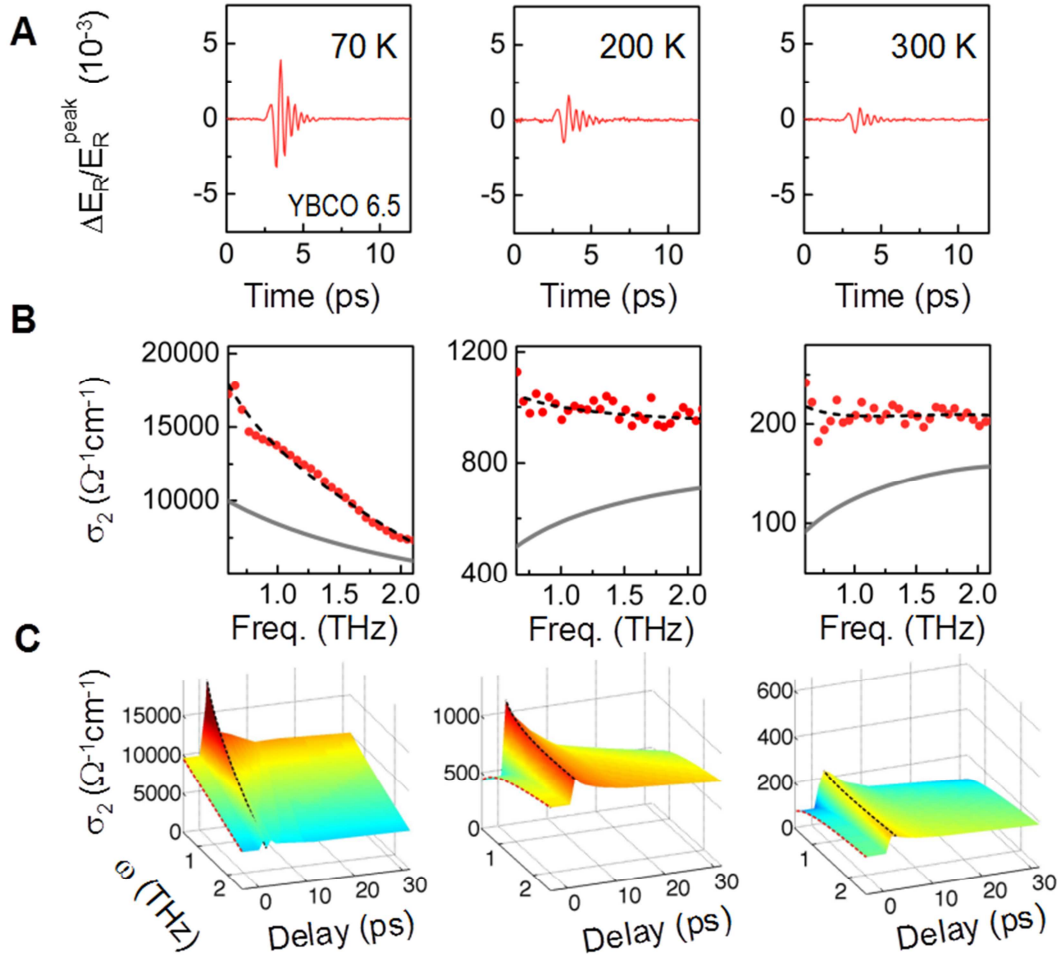


Figure 3. (A) Differential field reflectance ($\Delta E_R/E_R^{peak}$) in photo-stimulated YBCO 6.5, at three different temperatures above T_c (70 K, 200 K, 300 K), measured with THz pulses polarized along the a -axis (perpendicular to the CuO chains). The spectra are taken 2.5 ps after excitation with a 15 μm pulse polarized along the c -axis. (B) Imaginary part of the optical conductivity, σ_2 , as extracted from the amplitude- and phase-resolved reflectance using a multilayer model (see supplementary material S2 and S3). Black dashed lines are fits to the measured data with the function $\sigma_2(\omega) = \frac{D^{SF}}{\omega} + C + \sigma_2^0(\omega)$, where D^{SF} and C are frequency-independent constants that vary with time delay. The grey line shows $\sigma_2^0(\omega)$, the equilibrium conductivity at negative time delays^{xix}. (C) Time and frequency dependence of $\sigma_2(\omega, \tau)$.

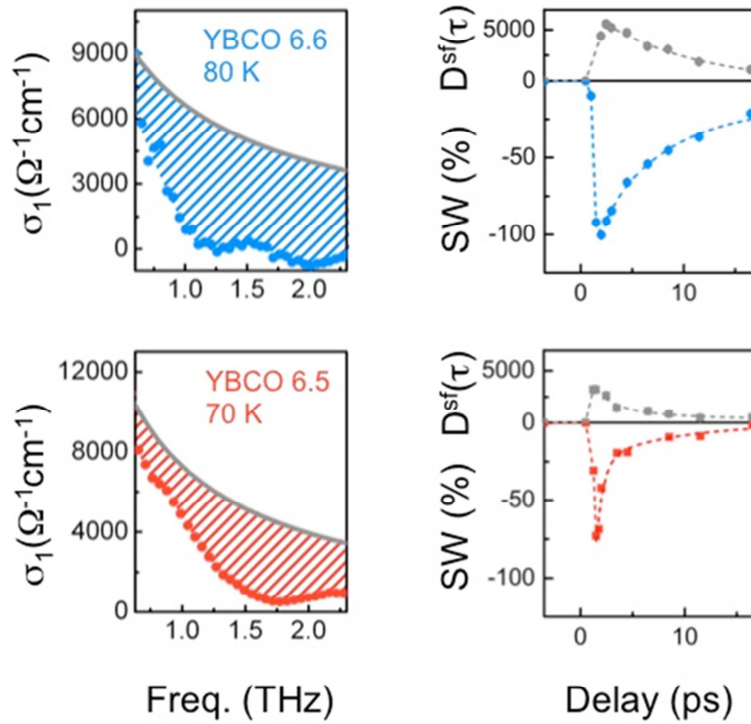


Figure 4. Real part of the optical conductivity, as measured in YBCO 6.6 (blue dots, upper left panel) and YBCO 6.5 (red dots, lower left panel). The measurements are performed at 2.5 ps pump-probe time delay. The grey curves are $\sigma_1(\omega)$ spectra determined at equilibrium^{xix}. The conductivity decreases from the equilibrium value (blue and red dashed regions), indicative of the opening of a gap. The time-dependent integrated spectral weight (blue squares in the upper right panel and red squares in the lower right panel) recovers in a few tens of picoseconds, the same timescale as the decay of the superfluid density in both compounds (grey squares).

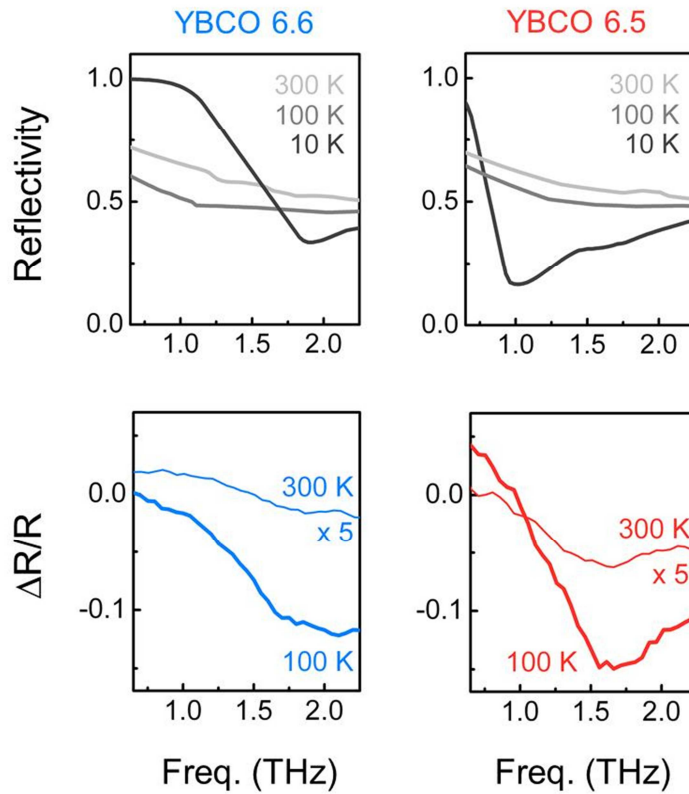


Figure 5. Upper panels. Equilibrium normal-incidence reflectivity for fields polarized along the c -axis (S1 and Refs. (xlii) and (xliv)). A featureless reflectivity is observed above T_c . Josephson plasma edges appear in the superconducting state. **Lower panels.** Light-induced changes in the normal-incidence reflectivity 2 ps after photo-excitation. Plasma edges appear near the frequency at which they are observed at equilibrium below T_c .

Superfluid Density

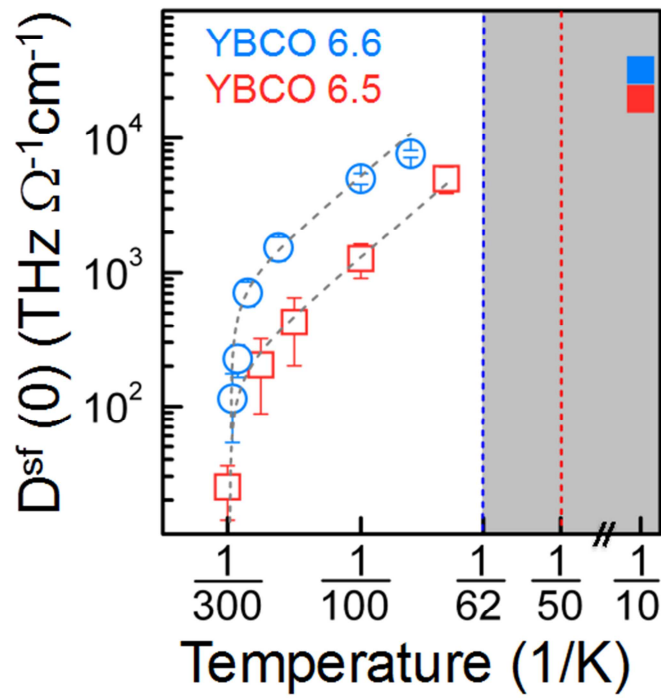


Figure 6A. Temperature dependence of the in-plane superfluid density, as extracted from the fits shown in Figures 2 and 3. An exponential decay in the superfluid density is observed in the low temperature range ($T < 200$ K), whilst a sharper decay, following a mean field type behavior (see text) is observed near room temperature.

Non Equilibrium Phase Diagram

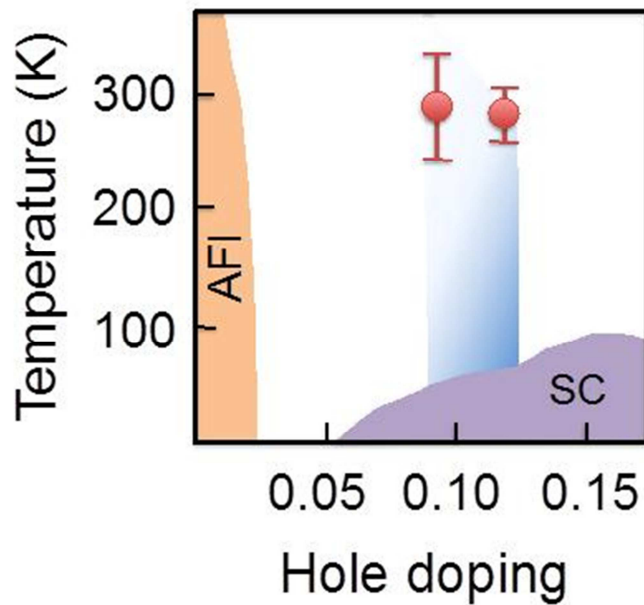


Figure 6B. Schematic representation of the region of phase diagram for which non-equilibrium light-induced superconductivity is observed (blue shaded region). AFI and SC indicate the antiferromagnetic insulating and the equilibrium superconducting phase, respectively. The red dots represent the results of the fit (Figure 6A), which indicate a nonzero light-induced superfluid density all the way to room temperature.

SUPPLEMENTARY INFORMATION (S1-S6)

S1 Sample Growth and Characterization

YBa₂Cu₃O_{7-δ} crystals of typical dimensions 2 x 2 x 1 mm³ were grown in Y-stabilized zirconium crucibles¹. The hole doping of the Cu-O planes was adjusted by controlling the oxygen content of the CuO chain layer δ by annealing in flowing O₂ and subsequent rapid quenching.

The T_c values ($T_c = 50$ K for YBCO 6.5 and $T_c = 62$ K for YBCO 6.6) were determined by dc magnetization measurements, as shown in Figure S1A. The measured superconducting transition was found to be sharp in both samples ($\Delta T_c \sim 2-4$ K).

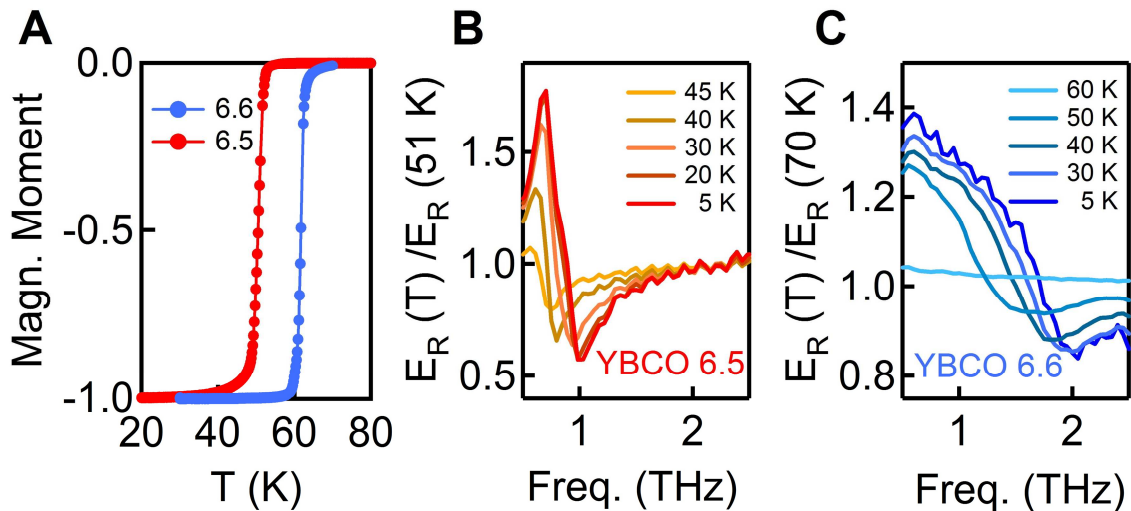


Figure S1. (A) SQUID characterization of the dc magnetization across the superconducting transition. (B) Josephson plasma resonance in the relative THz reflected field ratios for YBCO 6.5 and (C) YBCO 6.6 in the superconducting state.

¹ S. I. Schlachter, U. Tutsch, W. H. Fietz, *et al.*, "Pressure effect and specific heat of RBa₂Cu₃O_x at distinct charge carrier concentrations: Possible influence of stripes", *Int. J. Mod. Phys. B* **14**, 3673 (2000).

The static optical properties of the two crystals were also characterized by THz time-domain spectroscopy. Broadband THz pulses (0.5-2.5 THz) were focused onto the sample surface at 30° incidence, with polarization perpendicular to the Cu-O planes (i.e., parallel to the c -axis). The reflected electric field was measured by electro-optic sampling at different temperatures, below and above T_c .

Figure S1B and S1C show the absolute value of the frequency-dependent reflected electric field at a given temperature $|\tilde{E}_R(T)|$, normalized to the same quantity measured above T_c . In both materials, below T_c a strong edge appeared at a frequency ω_J . This feature corresponds to the Josephson plasma resonance. The frequency ω_J increased with decreasing temperature, reaching $\omega_J(T \rightarrow 0) \sim 0.8$ THz for YBCO 6.5 and $\omega_J(T \rightarrow 0) \sim 1.4$ THz for YBCO 6.6.

S2 In-plane optical properties (bulk approximation)

The procedure discussed in the present section is used to extract the transient optical properties from the transient electric-field reflectivity. This is valid without further corrections only if the volume photo-excited by the mid-infrared pulse is large compared to that probed by the THz pulse. This condition is fulfilled when probing in-plane, where the pump penetration depth, $d \sim 4$ μm , is always greater than the THz penetration depth, $L < 2$ μm . For out-of-plane probing, in which this approximation is not valid, see section S3.

At each mid-infrared pump / THz-probe time delay, the pump-induced change in reflected electric field $\Delta E_R(t) = E_R^{exc}(t) - E_R(t)$ was measured (see traces in Fig. 2 and 3, main text, upper panels and Fig. S2A, upper panel). The quantity $\Delta E_R(t)$ was acquired directly by filtering the electro-optic sampling signal with a lock-in amplifier, triggered by the signal from a mechanical chopper that modulated the mid-infrared pump. This measurement yielded “pump on” *minus* “pump off” reflected electric field. The unperturbed reflected electric field $E_R(t)$ was measured independently by placing the chopper on the THz beam (See Fig. S2A, lower panel).

This differential electric field $\Delta E_R(t)$ and the stationary reflected electric field $E_R(t)$ were independently Fourier transformed to obtain the complex valued frequency dependent $\Delta \tilde{E}_R(\omega)$ and $\tilde{E}_R(\omega)$.

The extrapolated zero-frequency spectral phases of these two complex quantities have a mutual offset. This offset is related to the fact that the position of the mechanical chopper can vary between the two measurements, the amplifier settings are different, and to the fact that $\Delta E_R(t)$ has typically a smaller signal-to-noise ratio than $E_R(t)$, leading to errors when the phase is extrapolated beyond the experimentally accessible spectral window (>0.5 GHz). This phase difference is corrected, subtracting a constant phase to bring both extrapolated zero-frequency phases to zero. The validity of this correction, which is a standard procedure in time domain THz spectroscopy², was further checked and confirmed in selected experiments in which the differential signal $\Delta E_R(t)$ was large enough to allow also for direct

² W. Withayachumnankul, H. Lin, S. P. Mickan, B. M. Fischer, and D. Abbott, “Analysis of Measurement Uncertainty in THz-TDS,” *Proceedings of SPIE* **6593**, 659326 (2007).

measurements of $E_R^{exc}(t)$ and $E_R(t)$ by chopping only the THz beam with and without pump.

The complex reflection coefficient of the photo-excited sample, $\tilde{r}'(\omega)$, was determined from the normalized pump-induced changes to the electric field $\Delta\tilde{E}_R(\omega)/\tilde{E}_R(\omega)$ (see Fig. S2B) using the relation,

$$\frac{\Delta\tilde{E}_R(\omega)}{\tilde{E}_R(\omega)} = \frac{\tilde{r}'(\omega) - \tilde{r}(\omega)}{\tilde{r}(\omega)},$$

where the stationary reflection coefficient $\tilde{r}(\omega)$ was calculated from the equilibrium optical properties (Ref. (xix) in the main text).

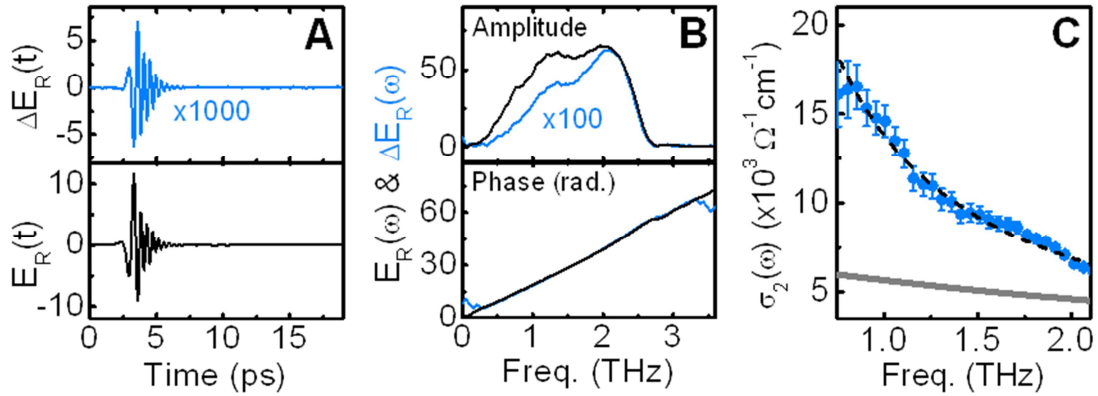


Figure S2. (A) The upper panel shows the pump-induced changes to the reflected THz field in YBCO 6.6 at 80 K, 2.5 ps after photo-excitation. The lower panel shows the corresponding reflected field without photo-excitation. The two panels have mutually consistent units. (B) Amplitudes of the Fourier transforms of the time traces (upper panel) and frequency dependent spectral phases after correction (lower panel). (C) Imaginary part of the conductivity, $\sigma_2(\omega)$, extracted with the procedure discussed in this section. The error bars indicate the propagated standard deviation from many scans of $\Delta E_R(t)$ and $E_R(t)$. The grey line is the equilibrium conductivity $\sigma_2^0(\omega)$, and the black dashed line is a fit to $\sigma_2(\omega) = \frac{D_{SF}}{\omega} + C + \sigma_2^0(\omega)$ (see Section S4).

From $\tilde{r}'(\omega)$, the complex refractive index $\tilde{n}(\omega)$ of the in-plane response was extracted using the Fresnel equation for the TE mode

$$\tilde{n}(\omega) = \left[\sin^2 \theta_0 + \cos^2 \theta_0 \left(\frac{1 - \tilde{r}'(\omega)}{1 + \tilde{r}'(\omega)} \right)^2 \right]^{1/2}.$$

The probe angle of incidence was $\theta_0 = 30^\circ$.

From the refractive index, the complex conductivity was extracted as

$$\tilde{\sigma}(\omega) = \frac{\omega}{4\pi i} [\tilde{n}(\omega)^2 - \varepsilon_\infty],$$

where $\varepsilon_\infty = 4.5$, a standard value for cuprates³.

S3 Out-of-plane optical properties (Inhomogeneous excitation)

The “bulk” model discussed in Section S2 is inappropriate when the pump penetration depth, d , is smaller than the probe penetration depth, L , as is the case of out-of-plane (c -axis) probing, ($d \sim 4 \mu\text{m}$, $L > 10 \mu\text{m}$).

Here we assume that the change in the complex refractive index is maximum at the sample surface, decaying exponentially with distance, z , from the surface toward its unperturbed bulk value, $\tilde{n}_0(\omega)$, following Beer’s law (see figure S4.1),

$$\tilde{n}(\omega, z) = \tilde{n}_0(\omega) + \Delta\tilde{n}(\omega)e^{-\alpha z},$$

³ D. van der Marel, H. J. A. Molegraaf, J. Zaanen, et al., “Quantum critical behaviour in a high- T_c superconductor,” *Nature* **425**, 271 (2003).

where the linear extinction coefficient is $\alpha = 1/d$.

We describe the optical properties of the inhomogeneously excited medium by assuming a stack of layers of vanishing thickness $\delta z \rightarrow 0$, where $\tilde{n}(z) = \text{constant}$ for each layer⁴. For a single layer, j , the characteristic matrix of the sample may be written as

$$M_j = \begin{pmatrix} \cos(k_j \tilde{n}_j \delta z) & -\frac{i}{p_j} \sin(k_j \tilde{n}_j \delta z) \\ -ip_j \sin(k_j \tilde{n}_j \delta z) & \cos(k_j \tilde{n}_j \delta z) \end{pmatrix} \rightarrow \begin{pmatrix} 1 & -\frac{i}{p_j} k_j \tilde{n}_j \delta z \\ -ip_j k_j \tilde{n}_j \delta z & 1 \end{pmatrix}.$$

Here, $p_j = \tilde{n}_j \cos \theta_j$ for a TE mode and $p_j = \cos \theta_j / \tilde{n}_j$ for a TM mode. The quantity k_j is defined as $k_j = k_0 \cos \theta_j$, where the probe wave number in vacuum is $k_0 = \omega/c$.

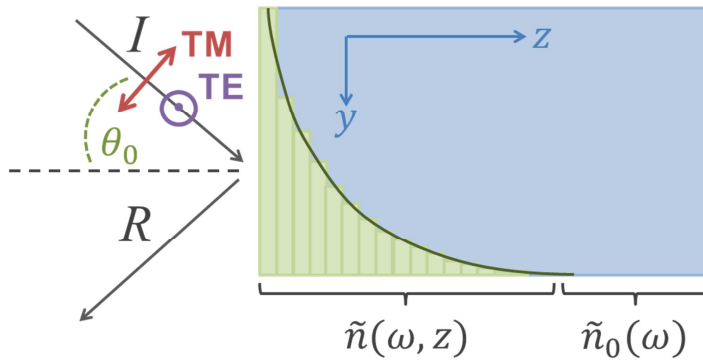


Figure S4.1. The refractive index of the excited crystal surface is approximated as a series of thin layers of constant $\tilde{n}(z)$. From layer to layer, the refractive index decays exponentially to the bulk value, $\tilde{n}_0(\omega)$. The incidence angle in the experiment is $\theta_0 = 30^\circ$.

⁴ M. Born and E. Wolf, "Principles of Optics," Pergamon Press.

The total characteristic matrix, M , is obtained as the product of the matrices for all layers, $M = \prod_{j=1}^N M_j$. In the continuum limit, and retaining only linear terms in δz , the characteristic matrix of the sample becomes

$$M \equiv \begin{pmatrix} 1 & -ik_0 \int_0^L g(\omega, z) dz \\ -ik_0 \int_0^L f(\omega, z) \left[1 - \left(\frac{\sin \theta_0}{\tilde{n}(\omega, z)} \right)^2 \right] dz & 1 \end{pmatrix},$$

where we define $f(\omega, z) = \tilde{n}(\omega, z)^2$ and $g(\omega, z) = 1$ for a TE mode, and $f(\omega, z) = 1$ and $g(\omega, z) = \tilde{n}(\omega, z)^2$ for a TM mode. From the elements of the characteristic matrix, m_{ij} , we can extract the reflection coefficient $r'(\omega)$,

$$r'(\omega) = \frac{(m_{11} + m_{12}p_L)p_1 - (m_{21} + m_{22}p_L)}{(m_{11} + m_{12}p_L)p_1 + (m_{21} + m_{22}p_L)}.$$

The quantity p_L is evaluated at the probe penetration depth and $p_1 = \cos \theta_0$ is calculated at the sample surface.

The equation for the reflection coefficient is not generally invertible such that one can solve analytically for $\tilde{n}(\omega)$. Instead we implement the Levenberg-Marquardt fitting algorithm in Matlab to extract the surface refractive index. The complex conductivity is calculated from $\tilde{n}(\omega)$ using the same method described in Section S2.

In figure 5 (main text), we display the appearance of a plasma edge by assuming normal-incidence reflection from a volume that is homogeneously transformed,

$$R(\omega) = \left| \frac{1 - \tilde{n}(\omega)}{1 + \tilde{n}(\omega)} \right|^2.$$

Figure S3.2 shows: (A) the re-calculated c -axis reflectivity, (B) real and (C) imaginary part of the conductivity.

As discussed in the main text, the photo-induced normal-incidence reflectivity displays a Josephson plasma edge at $\omega_J \sim 1$ THz. The complex conductivity is consistent with a photo-induced Josephson response, as $\sigma_1(\omega)$ is reduced and $\sigma_2(\omega)$ turns positive and increases at low frequencies below ω_J .

To connect these calculations with previous work, in figure S3.2 we show that the multilayer model agrees well with a model (Ref. (xxxi) in the main text), in which the system can be described as a single uniformly excited layer of thickness d on a semi-infinite, unperturbed bulk.

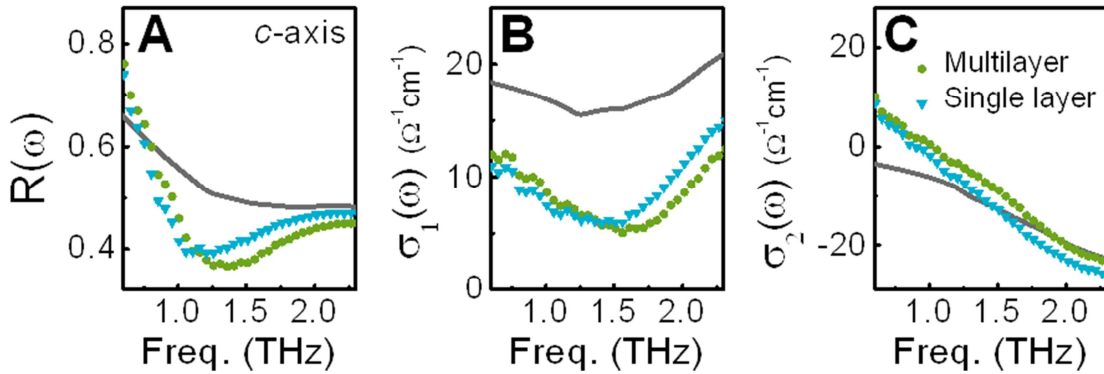


Figure S3.2. Transient out-of-plane optical properties of YBCO 6.5 at 100 K, 2 ps after photo-excitation. **(A)** Recalculated normal-incidence reflectivity obtained by simulating the exponential decay of the pump (green circles) and considering only a single excited layer (blue triangles). **(B)** Transient real part of the conductivity. **(C)** Transient imaginary part of the conductivity. The grey lines show the equilibrium optical properties extracted from Ref. (xliv) in the main text.

To further substantiate the validity and consistency of the multi-layer model and of our analysis, in figure S3.3 we show how in the opposite limit, such as that used to extract in-plane probing data, bulk model and multilayer model agree.

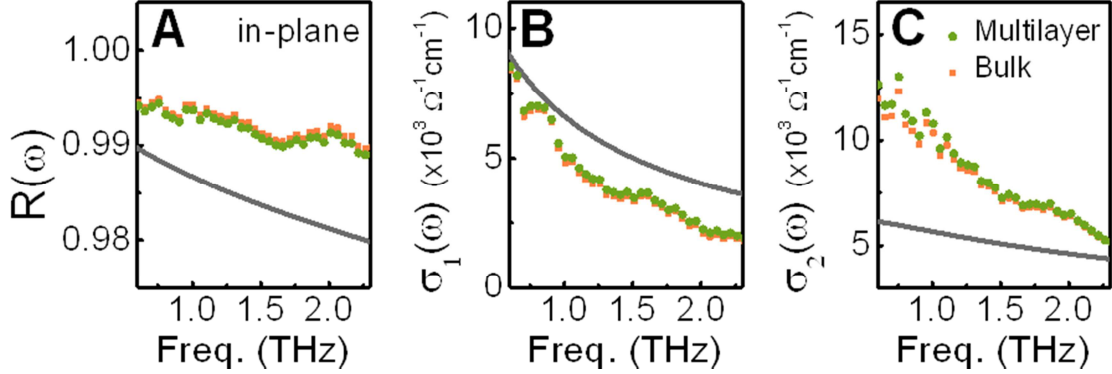


Fig. S3.3. Validity of bulk approximation for the in-plane optical properties. Recalculated normal-incidence reflectivity **(A)**, real conductivity **(B)**, and imaginary conductivity **(C)** for the transient in-plane optical properties of YBCO 6.6 at 100 K (figure 2 in the main text). The results of the multilayer model (green circles) agree well with those obtained using the bulk model (orange squares).

S4 Fit function for transient in-plane $\sigma_2(\omega, \tau)$

The fit function for the transient in-plane $\sigma_2(\omega, \tau)$ was determined by assuming a two-fluid scenario.

Firstly, we consider the excitation of a bath of incoherent quasi-particles, in which only a fraction of the electrons contributing to the optical properties could be turned superconducting. This leads to a functional form of the type

$$\sigma_2(\omega, \tau) = \frac{D_{SF}(\tau)}{\omega} + \sigma_2^0(\omega), \text{ for all time delays } \tau > 0. \text{ Here we denote } \sigma_2^0(\omega)$$

as the imaginary part of the conductivity of the unexcited material, and define $D_{SF}(\tau)$ as a quantity proportional to the superfluid density in the light

induced state, as extracted from the London equations in the low-frequency limit.

Secondly, as the mid-infrared field is expected to couple to other excitations as well, an additional term in the light induced state is required, taking into account the perturbed distribution of incoherent quasi-particles (which do not become superconducting) and the change in the spectrum of lattice vibrations.

To estimate this additional contribution, we fit the equilibrium complex conductivity at 200 K (non-superconducting), as extracted from data in Ref. (xix) in the main text, over a broad frequency range that includes the low frequency phonons by using an extended Drude model.

Three perturbations are considered.

(a) We consider the case in which the temperature of the incoherent quasi-particles is increased by the mid-infrared excitation (without changing their number). Such increase was simulated by changing the quasi-particle scattering rate Γ_{Drude} . This is analyzed in figure S4A, where for a fictitious 10% increase in Γ_{Drude} a decreased $\sigma_2(\omega)$ is found. Within the confidence of the experimental data, the low frequency behavior can be considered $\sigma_2^0(\omega) - constant$. A decrease of the scattering rate would result in a perturbed response of the type $\sigma_2^0(\omega) + constant$

(b) We also analyze the case for which either the number of incoherent quasi-particles is changed via inter-band excitations, or their effective mass is modified. This is simulated in terms of a 10% increase in the plasma frequency Ω_p of the electron gas. As shown in figure S4B, this leads to a low frequency response of the type $\sigma_2^0(\omega) + constant$.

(c) Finally, we consider the case in which all the phonon resonances are shifted by 10%. In this case, in the low frequency region, we estimate a perturbation that is nearly two orders of magnitude smaller than for perturbation of the quasi-particle spectrum in (a) and (b).

Based on this analysis, we chose a fitting function for the transient response

$$\text{of the type } \sigma_2(\omega, \tau) = \frac{D_{SF}(\tau)}{\omega} + C(\tau) + \sigma_2^0(\omega).$$

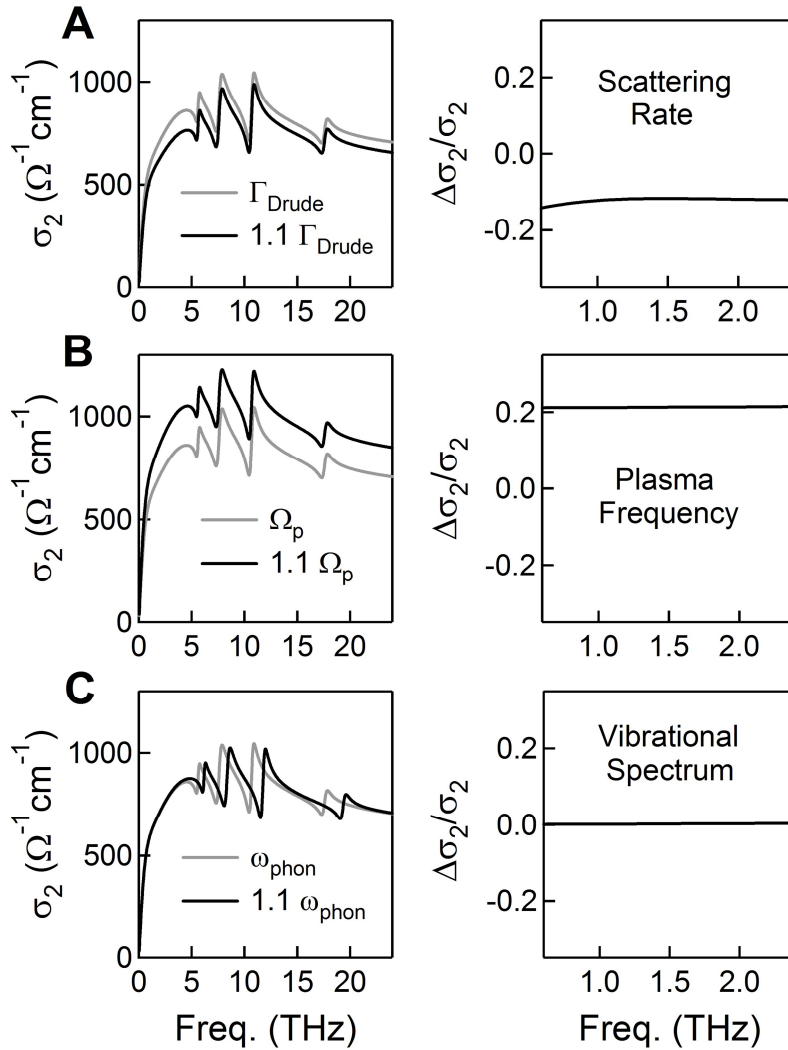


Figure S4. Estimated change in the imaginary conductivity for **(A)** a 10% increase in the quasi-particle scattering rate; **(B)** a 10% increase in the quasi-particle plasma frequency. **(C)** a 10% increase in the frequency of all phonon modes. In left panels broadband calculated $\sigma_2(\omega)$ spectra are displayed. Right panels show the low-frequency changes in $\sigma_2(\omega)$ induced by the 10% increase in the parameters.

S5 Temperature dependence of transient $\sigma_1(\omega)$

Figures S5A and S5B display the real part of the optical conductivity, $\sigma_1(\omega)$, in the photo-induced state of YBCO 6.5 and 6.6, respectively. The light-induced phases show large reduction in spectral weight when they are created at base temperatures near T_c (see also figure 4 in the main text).

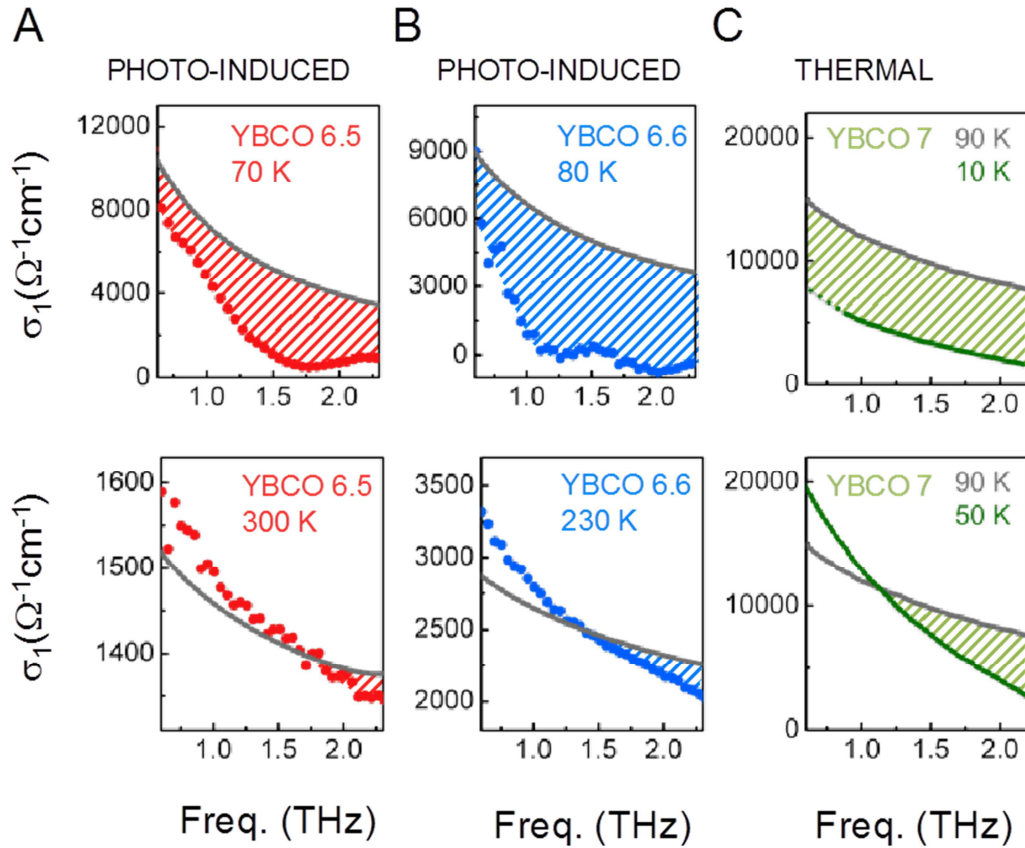


Fig. S5. Real part of the optical conductivity for **(A)** YBCO 6.5 (red) and **(B)** YBCO 6.6 (blue) in the equilibrium and photo-induced states, 2.5 ps after excitation. The measurements are performed at base temperatures about 20 K above (top row) and far above (bottom row) T_c . The grey lines show the equilibrium $\sigma_1(\omega)$. The shaded area shows the photo-induced loss of spectral weight in the gapped region at higher frequencies. **(C)** Fits to the equilibrium $\sigma_1(\omega)$ in the superconducting state of optimally doped YBCO 7 (from Ref. (5)). The grey line shows the normal state $\sigma_1(\omega)$ at 90 K. The conductivity displays complete gapping at 10 K (top) and partial gapping at high frequency at 50 K (bottom).

⁵ M.C. Nuss, P. M. Mankiewich, M. L. O'Malley, E. H. Westerwick, and P. B. Littlewood, "Dynamic Conductivity and "Coherence Peak" in $\text{YBa}_2\text{Cu}_3\text{O}_7$ Superconductors," *Phys. Rev. Lett.* **66**, 3305 (1991).

As the base temperature is increased, a spectral weight gain is observed in the photo-induced phase at low frequencies.

It is instructive to compare these observations with similar conductivity changes reported in YBCO 7 at equilibrium. For temperatures much less than T_c (10 K), where the superfluid density is highest, large spectral weight decreases are observed. On the other hand, nearer to T_c (50 K), where the superfluid density is lower, spectral weight is gained at the lowest frequencies.

S6 Estimate of the field-induced lattice displacement

The amplitude of the field-induced atomic displacement due to mid-infrared photo-excitation can be estimated assuming an ionic bonding between the apical O^{2-} ion and the Cu(1) ion in the CuO chains.

The atomic polarizability can be derived as $\mathbf{P}(\omega_0) = \epsilon_0 \chi(\omega_0) \mathbf{E}(\omega_0)$, where $\omega_0 = 20$ THz and $\|\mathbf{E}(\omega_0)\| \cong 2$ MV/cm. The susceptibility $\chi(\omega_0)$ is calculated from the c -axis equilibrium optical conductivity using $|\epsilon_0 \chi(\omega_0)| = \left| \frac{\sigma(\omega_0)}{\omega_0} \right|$. As $|\sigma_1(\omega_0)| \cong |\sigma_2(\omega_0)| \cong 30 \Omega^{-1} \text{cm}^{-1}$ (from Ref. (xlii) in the main text), one gets $|\epsilon_0 \chi(\omega_0)| \cong 2 \cdot 10^{-12} \Omega^{-1} \text{cm}^{-1} \text{s}$ and $\|\mathbf{P}(\omega_0)\| \cong 4 \cdot 10^{-6} \text{C} \cdot \text{cm}^{-2}$.

The average size of the photo-induced electric dipole, i.e., the displacement of the oxygen ions, is then given by $d = \|\mathbf{P}(\omega_0)\|/nQ$, where n is the density of dipoles (2 per unit cell of volume 173 \AA^3) and $Q = 3e$. This yields $d \sim 7$ pm, which is approximately 4% of the equilibrium Cu-O distance.

REFERENCES (Main text)

- ⁱ Z. A. Xu, N. P. Ong, Y. Wang, T. Kakeshita, and S. Uchida, „Vortex-like excitations and the onset of superconducting phase fluctuation in underdoped $\text{La}_{2-x}\text{Sr}_x\text{CuO}_4$,“ *Nature* **406**, 486 (2000).
- ⁱⁱ D.N. Basov and T. Timusk, “Electrodynamics of high-T-c superconductors,” *Rev. Mod. Phys.* **77**, 721 (2005).
- ⁱⁱⁱ A. Dubroka, M. Rössle, K. W. Kim, et al., “Evidence of a Precursor Superconducting Phase at Temperatures as High as 180 K in $\text{RBa}_2\text{Cu}_3\text{O}_{7-\delta}$ (R=Y,Gd,Eu) Superconducting Crystals from Infrared Spectroscopy,” *Phys. Rev. Lett.* **106**, 047006 (2011).
- ^{iv} V. J. Emery and S. A. Kivelson, "Importance of Phase Fluctuations in Superconductors with Small Superfluid Density," *Nature* **374**, 434 (1995).
- ^v E. Berg, D. Orgad, S.A. Kivelson, “Route to high temperature superconductivity in composite systems” *Phys. Rev. B* **78**, 094509 (2011).
- ^{vi} J. Hammer, M. Aprili, I. Petkovic, “Microwave Cooling of Josephson Plasma Oscillations,” *Phys. Rev. Lett.* **107**, 017001 (2011).
- ^{vii} M. Rini et al. “Control of the electronic phase of a manganite by mode-selective vibrational excitation” *Nature* **449**, 72 (2007).
- ^{viii} R. I. Tobey, D. Prabhakaran, A. T. Boothroyd, and A. Cavalleri, “Ultrafast Electronic Phase Transition in $\text{La}_{1/2}\text{Sr}_{3/2}\text{MnO}_4$ by Coherent Vibrational Excitation: Evidence for Nonthermal Melting of Orbital Order,” *Phys. Rev. Lett.* **101**, 197404 (2008).
- ^{ix} M. Först, C. Manzoni, S. Kaiser, et al., “Nonlinear phononics as an ultrafast route to lattice control,” *Nature Physics* **7**, 854 (2011)
- ^x J. Demsar, B. Podobnik, V. V. Kabanov, et al. "Superconducting Gap Δ_c , the Pseudogap Δ_p , and pair fluctuations above T_c in overdoped $\text{Y}_{1-x}\text{Ca}_x\text{Ba}_2\text{Cu}_3\text{O}_{7-\delta}$

from Femtosecond Time-Domain Spectroscopy," *Phys. Rev. Lett.* **82**, 4918 (1999).

^{xii} R. A. Kaindl, M. Woerner, T. Elsaesser, D. C. Smith, J. F. Ryan, G. A. Farnan, M. P. McCurry, and D. G. Walmsley, "Ultrafast Mid-Infrared Response of $\text{YBa}_2\text{Cu}_3\text{O}_{7-\delta}$," *Science* **287**, 470 (2000).

^{xiii} R. D. Averitt, G. Rodriguez, A. I. Lobad, J. L. W. Siders, S. A. Trugman, and A. J. Taylor, "Nonequilibrium superconductivity and quasiparticle dynamics in $\text{YBa}_2\text{Cu}_3\text{O}_{7-\delta}$," *Phys. Rev. B* **63**, 140502 (2001).

^{xiiii} N. Gedik, et al. "Abrupt Transition in Quasiparticle Dynamics at Optimal Doping in a Cuprate Superconductor System" *Phys. Rev. Lett.* **95**, 117005 (2005)

^{xiv} L. Perfetti, P.A. Loukakos, M. Lisowski et al. "Ultrafast electron relaxation in superconducting $\text{Bi}_2\text{Sr}_2\text{CaCu}_2\text{O}_{8+\delta}$ by time-resolved photoelectron spectroscopy," *Phys. Rev. Lett.* **99**, 197001 (2007).

^{xv} A. Pashkin, M. Porer, M. Beyer et al. "Femtosecond Response of Quasiparticles and Phonons in Superconducting $\text{YBa}_2\text{Cu}_3\text{O}_{7-\delta}$ Studied by Wideband Terahertz Spectroscopy" *Phys. Rev. Lett.* **105**, 067001 (2010).

^{xvi} S. Dal Conte, C. Giannetti, G. Coslovic et al. "Disentangling the electronic and phononic glue in a High T_c superconductor" *Science* **335**, 1600 (2012).

^{xvii} G. Yu, C. H. Lee, A. J. Heeger, N. Herron, and E. M. McCarron, "Transient photoinduced conductivity in single crystals of $\text{YBa}_2\text{Cu}_3\text{O}_{6.3}$: "Photodoping" to the metallic state," *Phys. Rev. Lett.* **67**, 2581 (1991).

^{xviii} G. Nieva, E. Osquiguil, J. Guimpel et al. "Photo-induced Enhancement of Superconductivity" *Appl. Phys. Lett.* **60**, 2159 (1992).

^{xix} J. Hwang, J. Yang, T. Timusk, et al., "a-axis optical conductivity of detwinned ortho-II $\text{YBa}_2\text{Cu}_3\text{O}_{6.50}$," *Phys. Rev. B* **73**, 014508 (2006).

^{xx} J.F. Annett, “Superconductivity, Superfluids and Condensates,” Oxford Master Series in Condensed Matter Physics, Oxford, 2004.

^{xxi} R. Kleiner, F. Steinmeyer, G. Kunkel, and P. Müller, “Intrinsic Josephson effects in $\text{Bi}_2\text{Sr}_2\text{CaCu}_2\text{O}_8$ single crystals,” *Phys. Rev. Lett.* **68**, 2394 (1992).

^{xxii} K. Tamakasu, Y. Nakamura, and S. Uchida, “Charge dynamics across the CuO_2 planes in $\text{La}_{2-x}\text{Sr}_x\text{CuO}_4$,” *Phys. Rev. Lett.* **69**, 1455 (1992).

^{xxiii} A.A. Tsvetkov, D. van der Marel, K.A. Moler et al. “Global and local measures of the intrinsic Josephson coupling in $\text{Tl}_2\text{Ba}_2\text{CuO}_6$ as a test of the interlayer tunnelling model,” *Nature* **395**, 360 (1998).

^{xxiv} D. N. Basov, T. Timusk, B. Dabrowski, and J. D. Jorgensen, “c-axis response of $\text{YBa}_2\text{Cu}_4\text{O}_8$: A pseudogap and possibility of Josephson coupling of CuO_2 planes,” *Phys. Rev. B* **50**, 3511 (1994).

^{xxv} Y. S. Lee, Kouji Segawa, Z. Q. Li, et al., “Electrodynamics of the nodal metal state in weakly doped high-Tc cuprates,” *Phys. Rev. B* **72**, 054529 (2005).

^{xxvi} D. Einzel and I. Schürerer, “Weak Coupling Theory of Clean (d+s)-Wave Superconductors,” *Journal of Low Temperature Physics* **117**, 15 (1999).

^{xxvii} R. Prozorov, “Superfluid Density in a superconductor with an extended d-wave gap,” *Supercond. Sci. Technol.* **21**, 082003 (2008).

^{xxviii} T. Dahm, P. J. Hirschfeld, D. J. Scalapino, and L. Zhu, “Nodal quasiparticle lifetime in cuprate superconductors,” *Phys. Rev. B* **72**, 214512 (2005).

^{xxix} D. D. Prokof'ev, M. P. Volkov, and Yu. A. Boëkov, “Pseudogap and Its Temperature Dependence in YBCO from the Data of Resistance Measurements,” *Physics of the Solid State* **45**, 1223 (2003).

^{xxx} R.V. Vovk, M.A. Obolenskii, A.A. Zavgorodniy, D.A. Lotnyk, K.A. Kotvitskaya, “Temperature dependence of the pseudogap in aluminum and praseodymium-doped $\text{YBa}_2\text{Cu}_3\text{O}_{7-d}$ single crystals,” *Physica B* **404**, 3516 (2009).

xxxii D. Fausti, R. I. Tobey, N. Dean. et al. "Light induced superconductivity in a striped ordered cuprate" *Science* **331**, 189 (2011).

xxxiii A. D. Caviglia, R. Scherwitzl, P. Popovich, et al., "Ultrafast Strain Engineering in Complex Oxide Heterostructures," *Phys. Rev. Lett.* **108**, 136801 (2012)

xxxiiii M. Först, R.I. Tobey, S.Wall et al., "Driving magnetic order in a manganite by ultrafast lattice excitation," *Phys. Rev. B* **84**, 241104(R) (2011)

xxxv J.A. Slezak, J. Lee, M. Wang et al. „Imaging the impact on cuprate superconductivity of varying the interatomic distances within individual crystal unit cells“ *Proc. Nat’l Acad. Scie. USA* **105**, 3203 (2008).

xxxvi E. Pavarini, I. Dasgupta, T. Saha-Dasgupta, et al., "Band-Structure Trend in Hole-Doped Cuprates and Correlation with T_{cmax} ," *Phys. Rev. Lett.* **87**, 047003 (2001).

xxxvii C. Weber, K. Haule, and G. Kotliar, "Apical oxygens and correlation strength in electron- and hole-doped copper oxides," *Phys. Rev. B* **82**, 125107 (2010).

xxxviii M. Mori, G. Khaliullin, T. Tohyama, S. Maekawa „Origin of the spatial variation of the pairing gap in Bi-based High Temperature Cuprate Superconductors“ *Phys. Rev. Lett.* **101**, 247003 (2008).

xxxix P.L. Kapitza, "Dynamic stability of a pendulum with an oscillating point of suspension," *Zh. Eksp. Teor. Fiz.* **21**, 588 (1951)

xl L.D. Landau and E.M. Lifschitz *Mechanics* (Pergamon, Oxford 1976)

xli A.W. Overhauser, "Polarization of Nuclei in Metals," *Phys. Rev.* **92**, 411 (1953).

xlii G. Calestani and C. Rizzoli, "Crystal structure of the $YBa_2Cu_3O_7$ superconductor by single-crystal X-ray diffraction," *Nature* **328**, 606 (1987).

^{xlii} C.C. Homes, T. Timusk, D. A. Bonn, R. Liang, and W.N. Hardy, "Optical phonons polarized along the c axis of $\text{YBa}_2\text{Cu}_3\text{O}_{6+x}$, for $x = 0.5$ to 0.95 ," *Can. J. Phys.* **73**, 663 (1995).

^{xliii} G. Burns, F.H. Dacol, P.P. Freitas, et al., "Phonons in $\text{YBa}_2\text{Cu}_3\text{O}_{7-\delta}$ -type materials," *Phys. Rev. B* **37**, 5171 (1988).

^{xliv} C. C. Homes, T. Timusk, D. A. Bonn, et al., "Optical properties along the c-axis of $\text{YBa}_2\text{Cu}_3\text{O}_{6+x}$, for $x=0.5$ to 0.95 : evolution of the pseudogap," *Physica C* **254**, 265 (1995).